Progress In Electromagnetics Research, Vol. 142, 485–503, 2013

AN IMPULSE SAMPLING APPROACH FOR EFFICIENT 3D TLM-BASED ADJOINT SENSITIVITY ANALYSIS

Osman S. Ahmed*, **Mohamed H. Bakr, and Xun Li**

Department of Electrical and Computer Engineering, McMaster University, Hamilton, ON L8S 4K1, Canada

Abstract—We present a memory efficient algorithm for the estimation of adjoint sensitivities with the transmission line modeling (TLM) method. Our algorithm manipulates the local scattering matrices to drastically reduce the required storage for problems with lossy dielectric discontinuities. Only one impulse per cell is stored for two dimensional simulations and three impulses per cell are stored for three dimensional simulations. The required memory storage for our impulse sampling approach is only 10% of of the original TLM-based adjoint sensitivity analysis. The technique is illustrated through two examples including the sensitivity analysis of a dielectric resonator antenna.

1. INTRODUCTION

Accurate design optimization of high frequency structures requires full wave 3D electromagnetic simulations. The optimization algorithm drives the simulator to carry out a number of iterations until the response meets the required design specifications. Gradient-based optimization techniques are robust tools in design optimization [1]. They require, however, sensitivity estimates that are classically obtained through finite differences. These approaches can have a significant computational overhead.

The Adjoint variable method (AVM) has been proposed for the acceleration of derivative-based optimization of microwave devices [2–8]. AVM allows for the estimation of the sensitivities of a given objective function with respect to all parameters using at most one extra simulation. AVM approaches can be contrasted with finite difference approaches, where at least N extra simulations are calculated, for a problem with N parameters.

Received 28 June 2013, Accepted 13 August 2013, Scheduled 13 September 2013

* Corresponding author: Osman S. Ahmed (mohammos@mcmaster.ca).

The AVM approach has been successfully developed for both time and frequency domain numerical techniques, including the finite difference time domain (FDTD) [8], the time-domain transmission line modeling (TLM) [7], the frequency domain transmission line modeling (FDTLM) [9], the method of moments (MOM) [10], and the finite element method (FEM) [11]. An efficient self AVM (SAVM) approach is developed for network parameter sensitivity analysis where the sensitivities are calculated without any extra simulations [12].

TLM-based AVM is memory intensive. The algorithm stores the incident impulses at all perturbed cells at all the time steps for both the original and adjoint simulations. Using a 3D Symmetric Condensed Node (SCN) [13, 14] to model problems with dielectric materials, at least 15 incident impulses are stored per perturbed cell for every time step in both the original and adjoint simulations [15]. This may make the TLM-based AVM approach infeasible for problems with large dielectric discontinuities where the field information is stored all over the discontinuity at every time instant.

In this paper, we present an approach that reduces the significant memory requirements for 3D TLM-based AVM calculations. We develop a formulation that requires only 10% of the memory storage required by the original TLM-based AVM technique. Through utilizing an elegant mathematical theory, the scattering matrix of each cell is factorized in a way that reduces the number of stored impulses. The adjoint variables are redefined to eliminate the memory requirements during the adjoint simulation. We extend the 2D theory presented in [6] to full 3D time-intensive simulations. Our novel theory is utilized for sensitivity analysis of 3D antenna problems which demonstrate the accuracy and efficiency of our approach.

This paper is organized as follows. The theory of TLM-based AVM is briefly reviewed in Section 2. The impulse sampling approach for the 3D-TLM adjoint sensitivity analysis is introduced in Section 3. Section 4 is dedicated for the numerical results where two examples illustrate the accuracy of our memory efficient approach. Our work is concluded in Section 5.

2. AVM THEORY FOR TLM

The TLM method is based on mapping electric and magnetic fields to electrical voltage and current quantities. The propagation of the electromagnetic waves is modeled through a network of transmission lines whose per length parameters (resistance, capacitance, and inductance) are functions of the discretization and the field constitutive parameters. The technique carries out a sequence of scattering and

connection steps of the voltage impulses incident on the transmission lines [14]. A complete time step of a TLM problem with non-dispersive boundaries is given by [14]:

$$\mathbf{V}_{k+1} = \mathbf{CSV}_k + \mathbf{V}_k^s \tag{1}$$

where $\mathbf{V}_k \in R^Q$ is the vector of incident impulses for all links at the kth time step. Here, $Q = N \times L$ is the total number of links inside the computational domain, where L is the number of transmission line links per cell and N is the total number of cells. The matrix $\mathbf{S} \in R^{Q\times Q}$ is a block diagonal matrix whose jth diagonal component, $\mathbf{S}^j \in R^{L\times L}$, is the scattering matrix of the jth cell. The matrix $\mathbf{C} \in R^{Q\times Q}$ is the overall connection matrix that connects reflected voltage impulses between different transmission lines and boundaries. The vector $\mathbf{V}_k^s$ is the vector of source excitation at the kth time step. In TLM, the scattered voltage impulses associated with each cell are calculated during the entire simulation time.

A general time domain objective function may be given by [7]:

$$F = \int_0^{T_m} \int_\Omega \psi(\mathbf{p}, \mathbf{V}) d\Omega dt = \int_0^{T_m} \Psi(\mathbf{p}, \mathbf{V}) dt \tag{2}$$

where Ω is the observation domain and T_m is the simulation time. $\psi(\mathbf{p}, \mathbf{V})$ is the local response function, $\mathbf{p}$ is the vector of optimization parameters and $\mathbf{V}$ is the continuous vector of $\mathbf{V}_k$. For lossy dielectric discontinuities, the sensitivity of F with respect to all the design parameters p_i, where $i = 1, \ldots, n$, can be efficiently calculated using the AVM approach using at most one extra simulation [15]. The AVM sensitivities are given by:

$$\frac{\partial F}{\partial p_i} = \frac{\partial^e F}{\partial p_i} - \sum_k \sum_j \boldsymbol{\lambda}_{j,k}^T \boldsymbol{\eta}_{j,k}^i, \quad i = 1, 2, \ldots, N \tag{3}$$

where $\partial^e / \partial p_i$ denotes the explicit dependence of the optimization function on the design parameters. The vector $\boldsymbol{\lambda}_{j,k}$ is the adjoint response of the jth affected cell at the kth time step. It is obtained at all the time steps through the backward-running adjoint system [15]:

$$\boldsymbol{\lambda}_{k-1} = \mathbf{S}^T \mathbf{C}^T \boldsymbol{\lambda}_k - \mathbf{V}_k^{s,\lambda}, \quad \boldsymbol{\lambda}(T_m) = 0 \tag{4}$$

where $\mathbf{V}_k^{s,\lambda} = \Delta t (\partial \Psi / \partial \mathbf{V})_{t=k\Delta t}$ is the adjoint excitation. The term $\boldsymbol{\eta}_{j,k}^i$ is obtained from the original simulation and is given by:

$$\boldsymbol{\eta}_{j,k}^i = \mathbf{C}^j \frac{\partial \mathbf{S}^j}{\partial p_i} \mathbf{V}_k^j. \tag{5}$$

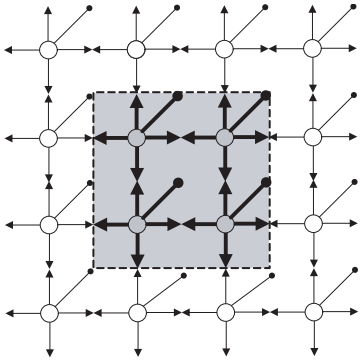

Figure 1. Illustration of the link storage for the regular TLM based AVM. The arrowed bold links are the ones for which $\boldsymbol{\eta}^i_{j,k}$ has nonzero components for a perturbation in the material parameters in the shadowed region.

Formula (4) represents a backward-running TLM simulation with a predetermined excitation. In this simulation, the connection process is performed before the scattering process. From (3) and (5), one can see that the adjoint variable $\boldsymbol{\lambda}$ is stored only at the transmission lines where the derivative of the scattering matrix $\mathbf{S}$ with respect to any of the design parameters is non-zero. The same backward running adjoint simulation is used for the calculation of the objective function sensitivities with respect to all the designable parameters.

The TLM-based AVM approach requires the storage of all perturbed links voltages in both the original and adjoint simulation (see Fig. 1 for the 2D case). For parameters associated with dielectric discontinuities, the number of extra storage is $2 \times L \times M$ per time step, where M is the number of perturbed TLM cells. The minimum number of links (L) per cell for modeling lossy dielectrics is 5 for 2D-TLM, 15 for 3D-TLM using the symmetrical condensed node (SCN) [13], and 12 for the 3D-TLM using the symmetrical super condensed node (SSCN) [16]. This implies significant memory storage for problems with large dielectric discontinuities, where it is required to estimate the sensitivities relative to the material properties or dimensions of the discontinuity.

3. THE IMPULSE SAMPLING APPROACH

Enhancement of the memory requirement of the TLM-based AVM can be achieved through careful manipulation of the system matrix $\mathbf{A}$=$\mathbf{CS}$

and its derivatives with respect to the designable parameters. First, the nodal scattering matrix $\mathbf{S}^j$ at each cell is expanded as the sum of two matrices:

$$\mathbf{S}^j = \mathbf{T}^j - \mathbf{P}^j, \tag{6}$$

where $\mathbf{T}^j \in R^{L\times L}$ is a parameter-dependent transmission matrix and $\mathbf{P}^j \in R^{L\times L}$ is a constant matrix that is independent of the optimization variables. Due to the symmetry of link contributions for each cell, the matrix $\mathbf{T}^j$ can be divided into 3 sub-matrices each with identical rows. Each sub-matrix is associated with a distinct field polarization;

$$\mathbf{T}^j = \begin{bmatrix} \mathbf{T}_x^j \\ \mathbf{T}_y^j \\ \mathbf{T}_z^j \end{bmatrix}. \tag{7}$$

By calculating the derivative of each sub-matrix with respect to the design parameters we can show that:

$$\frac{\partial \mathbf{T}^j}{\partial p_i}\mathbf{V}_k^j = \begin{bmatrix} \zeta_{x,j,k}^i \mathbf{1} \\ \zeta_{y,j,k}^i \mathbf{1} \\ \zeta_{z,j,k}^i \mathbf{1} \end{bmatrix}, \tag{8}$$

where $\zeta_{x,j,k}^i$, $\zeta_{y,j,k}^i$, and $\zeta_{z,j,k}^i$ are scalar quantities, and $\mathbf{1} \in R^{L/3}$ is a vector of ones. Using (5) and (8), we see that only three values are to be stored for each cell at each time step (see Fig. 2 for the 2D case).

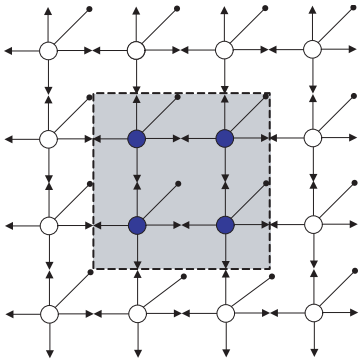

Figure 2. Illustration of the storage for the impulse sampling TLM based AVM. The colored circled cells are the ones for which $\partial\mathbf{T}/\partial p_i$ has nonzero components for a perturbation in the material parameters in the shadowed region.

This reduces the storage required for the original impulses by 80%. The vector of the adjoint variables $\boldsymbol{\lambda}_{j,k}$ is also split into three sub-vectors based on the three polarizations. A costless swapping operation is utilized to redefine the vector of adjoint variables as:

$$\tilde{\boldsymbol{\lambda}}_k^T = \boldsymbol{\lambda}_k^T \mathbf{C} \tag{9}$$

By substitution from (8) and (9) into (3), the AVM sensitivities are calculated using:

$$\frac{\partial F}{\partial p_i} = -\sum_k \sum_j \left(\zeta^i_{x,j,k} \mu^i_{x,j,k} + \zeta^i_{y,j,k} \mu^i_{y,j,k} + \zeta^i_{z,j,k} \mu^i_{z,j,k} \right) \tag{10}$$

where $\mu^i_{x,j,k}$, $\mu^i_{y,j,k}$, and $\mu^i_{z,j,k}$ are quantities derivable from the adjoint variables. Using (10), we calculate the sensitivities on the fly without any extra storage during the adjoint simulation. The vector summation in (3) is converted to the scalar summation (10). This implies more saving in the computational time of the algorithm. This approach achieves a maximum memory requirement of 10% of that utilized in the original TLM-based AVM approach [15].

We illustrate the details of the factorization (6) for the symmetric condensed node (SCN) widely used for 3D problems. In the following discussion, we drop the nodal superscript j for clarity. The nodal scattering matrix associated with the SCN can be formulated as [13]

$$\mathbf{S} = \begin{pmatrix}
a & b & d & 0 & 0 & 0 & 0 & 0 & b & 0 & -d & c & g & 0 & 0 \\
b & a & 0 & 0 & 0 & d & 0 & 0 & c & -d & 0 & b & g & 0 & 0 \\
d & 0 & a & b & 0 & 0 & 0 & b & 0 & 0 & c & -d & 0 & g & 0 \\
0 & 0 & b & a & d & 0 & -d & c & 0 & 0 & b & 0 & 0 & g & 0 \\
0 & 0 & 0 & d & a & b & c & -d & 0 & b & 0 & 0 & 0 & 0 & g \\
0 & d & 0 & 0 & b & a & b & 0 & -d & c & 0 & 0 & 0 & 0 & g \\
0 & 0 & 0 & -d & c & b & a & d & 0 & b & 0 & 0 & 0 & 0 & g \\
0 & 0 & b & c & -d & 0 & d & a & 0 & 0 & b & 0 & 0 & g & 0 \\
b & c & 0 & 0 & 0 & -d & 0 & 0 & a & d & 0 & b & g & 0 & 0 \\
0 & -d & 0 & 0 & b & c & b & 0 & d & a & 0 & 0 & 0 & 0 & g \\
-d & 0 & c & b & 0 & 0 & 0 & b & 0 & 0 & a & d & 0 & g & 0 \\
c & b & -d & 0 & 0 & 0 & 0 & 0 & b & 0 & d & a & g & 0 & 0 \\
e & e & 0 & 0 & 0 & 0 & 0 & 0 & e & 0 & 0 & e & h & 0 & 0 \\
0 & 0 & e & e & 0 & 0 & 0 & e & 0 & 0 & e & 0 & 0 & h & 0 \\
0 & 0 & 0 & 0 & e & e & e & 0 & 0 & e & 0 & 0 & 0 & 0 & h
\end{pmatrix} \tag{11}$$

where a, b, c, d, e, g, and h are general functions of the material local constitutive parameters and can be calculated as in [13]. The scattering matrix, in its current form, requires the storage of extra 15 local variables per cell in the perturbed domain at every time step. This

memory overhead is prohibitive, which limits the maximum allowed perturbation size in the computational domain.

3.1. Polarization-based Factorization

We utilize a modified numbering scheme to reorder the scattering matrix entries correspond to transmission line ports. This scheme is based on the polarization dependence of the transmission line ports, similar to [17]. In Fig. 3, the symmetrical condensed node is updated according to the proposed numbering scheme. The updated numbering scheme ensures simple and direct factorization of the scattering matrix according to the associated polarization. For example, in (11), $[V_1\ V_2\ V_9\ V_{12}\ V_{13}]^T$ are the voltage ports corresponding to the x-polarized electric field E_x. We transform these ports to be named $[V_1\ V_2\ V_3\ V_4\ V_5]^T$ as shown in Fig. 3. Similarly for the y polarization, the ports $[V_3\ V_4\ V_8\ V_{11}\ V_{14}]^T$ are transformed to $[V_6\ V_7\ V_8\ V_9\ V_{10}]^T$. Finally, for the z polarization, the ports $[V_5\ V_6\ V_7\ V_{10}\ V_{15}]^T$ are numbered as $[V_{11}\ V_{12}\ V_{13}\ V_{14}\ V_{15}]^T$. We then split the scattering matrix of the renumbered ports into three sub-matrices. Each sub-matrix contains the scattering coefficients for a group of ports that share the same polarization. The scattering matrix is then put in the form:

$$\mathbf{S} = \begin{pmatrix} \mathbf{S}_x \\ \mathbf{S}_y \\ \mathbf{S}_z \end{pmatrix} \tag{12}$$

where the scattering sub-matrices $\mathbf{S}_x$, $\mathbf{S}_y$ and $\mathbf{S}_z$ are given as

$$\mathbf{S}_x = \begin{pmatrix} a & b & b & c & g & d & 0 & 0 & -d & 0 & 0 & 0 & 0 & 0 & 0 \\ b & a & c & b & g & 0 & 0 & 0 & 0 & 0 & 0 & d & 0 & -d & 0 \\ b & c & a & b & g & 0 & 0 & 0 & 0 & 0 & 0 & -d & 0 & d & 0 \\ c & b & b & a & g & -d & 0 & 0 & d & 0 & 0 & 0 & 0 & 0 & 0 \\ e & e & e & e & h & 0 & 0 & 0 & 0 & 0 & 0 & 0 & 0 & 0 & 0 \end{pmatrix} \tag{13}$$

$$\mathbf{S}_y = \begin{pmatrix} d & 0 & 0 & -d & 0 & a & b & b & c & g & 0 & 0 & 0 & 0 & 0 \\ 0 & 0 & 0 & 0 & 0 & b & a & c & b & g & d & 0 & -d & 0 & 0 \\ 0 & 0 & 0 & 0 & 0 & b & c & a & b & g & -d & 0 & d & 0 & 0 \\ -d & 0 & 0 & d & 0 & c & b & b & a & g & 0 & 0 & 0 & 0 & 0 \\ 0 & 0 & 0 & 0 & 0 & e & e & e & e & h & 0 & 0 & 0 & 0 & 0 \end{pmatrix} \tag{14}$$

$$\mathbf{S}_z = \begin{pmatrix} 0 & 0 & 0 & 0 & 0 & 0 & d & -d & 0 & 0 & a & b & c & b & g \\ 0 & d & -d & 0 & 0 & 0 & 0 & 0 & 0 & 0 & b & a & b & c & g \\ 0 & 0 & 0 & 0 & 0 & 0 & -d & d & 0 & 0 & c & b & a & b & g \\ 0 & -d & d & 0 & 0 & 0 & 0 & 0 & 0 & 0 & b & c & b & a & g \\ 0 & 0 & 0 & 0 & 0 & 0 & 0 & 0 & 0 & 0 & e & e & e & e & h \end{pmatrix} \tag{15}$$

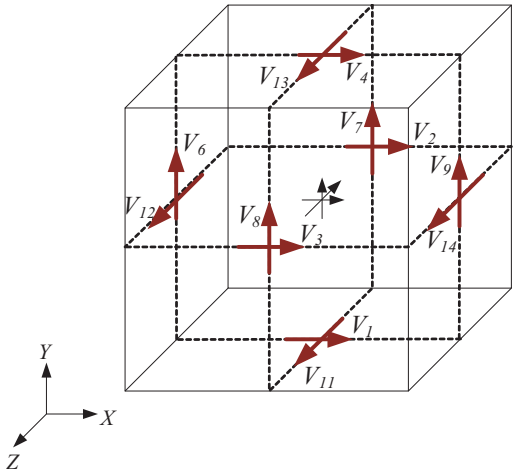

Figure 3. The space representation in TLM by the Symmetrical Condensed Node (SCN) with a revised port numbering.

3.2. Parameter-based Reduction

The scattering matrix entries a, b, c, d, e, g, and h depend on the local material properties as given in [13]. From [13], we can show that for $b = f_{3d}(\mathbf{p})$, we get $a = f_{3d}(\mathbf{p}) - 1/2$, $c = f_{3d}(\mathbf{p}) - 1/2$, $d = 1/2$ and $e = f_{3d}(\mathbf{p})$. For $g = g_{3d}(\mathbf{p})$, we get $h = g_{3d}(\mathbf{p}) - 1$ [13]. The x, y, and z scattering matrices can thus be factorized, similar to (6), to give:

$$\begin{aligned} \mathbf{S}_x &= \mathbf{T}_x - \mathbf{P}_x \\ \mathbf{S}_y &= \mathbf{T}_y - \mathbf{P}_y \\ \mathbf{S}_z &= \mathbf{T}_z - \mathbf{P}_z \end{aligned} \tag{16}$$

where the factorization matrices are given by:

$$\mathbf{P}_x = \frac{1}{2}\begin{pmatrix} 1 & 0 & 0 & 1 & 0 & -1 & 0 & 0 & 1 & 0 & 0 & 0 & 0 & 0 & 0 \\ 0 & 1 & 1 & 0 & 0 & 0 & 0 & 0 & 0 & 0 & 0 & -1 & 0 & 1 & 0 \\ 0 & 1 & 1 & 0 & 0 & 0 & 0 & 0 & 0 & 0 & 0 & 1 & 0 & -1 & 0 \\ 1 & 0 & 0 & 1 & 0 & 1 & 0 & 0 & -1 & 0 & 0 & 0 & 0 & 0 & 0 \\ 0 & 0 & 0 & 0 & 1 & 0 & 0 & 0 & 0 & 0 & 0 & 0 & 0 & 0 & 0 \end{pmatrix}, \tag{17}$$

$$\mathbf{T}_x = \begin{pmatrix} b & b & b & b & g & 0 & 0 & 0 & 0 & 0 & 0 & 0 & 0 & 0 & 0 \\ b & b & b & b & g & 0 & 0 & 0 & 0 & 0 & 0 & 0 & 0 & 0 & 0 \\ b & b & b & b & g & 0 & 0 & 0 & 0 & 0 & 0 & 0 & 0 & 0 & 0 \\ b & b & b & b & g & 0 & 0 & 0 & 0 & 0 & 0 & 0 & 0 & 0 & 0 \\ b & b & b & b & g & 0 & 0 & 0 & 0 & 0 & 0 & 0 & 0 & 0 & 0 \end{pmatrix}, \tag{18}$$

$$\mathbf{P}_y = \frac{1}{2}\begin{pmatrix} -1 & 0 & 0 & 1 & 0 & 1 & 0 & 0 & 1 & 0 & 0 & 0 & 0 & 0 & 0 \\ 0 & 0 & 0 & 0 & 0 & 0 & 1 & 1 & 0 & 0 & -1 & 0 & 1 & 0 & 0 \\ 0 & 0 & 0 & 0 & 0 & 0 & 1 & 1 & 0 & 0 & 1 & 0 & -1 & 0 & 0 \\ 1 & 0 & 0 & -1 & 0 & 1 & 0 & 0 & 1 & 0 & 0 & 0 & 0 & 0 & 0 \\ 0 & 0 & 0 & 0 & 0 & 0 & 0 & 0 & 0 & 1 & 0 & 0 & 0 & 0 & 0 \end{pmatrix}, \tag{19}$$

$$\mathbf{T}_y = \begin{pmatrix} 0 & 0 & 0 & 0 & 0 & b & b & b & b & g & 0 & 0 & 0 & 0 & 0 \\ 0 & 0 & 0 & 0 & 0 & b & b & b & b & g & 0 & 0 & 0 & 0 & 0 \\ 0 & 0 & 0 & 0 & 0 & b & b & b & b & g & 0 & 0 & 0 & 0 & 0 \\ 0 & 0 & 0 & 0 & 0 & b & b & b & b & g & 0 & 0 & 0 & 0 & 0 \\ 0 & 0 & 0 & 0 & 0 & b & b & b & b & g & 0 & 0 & 0 & 0 & 0 \end{pmatrix}, \tag{20}$$

$$\mathbf{P}_z = \frac{1}{2}\begin{pmatrix} 0 & 0 & 0 & 0 & 0 & 0 & -1 & 1 & 0 & 0 & 1 & 0 & 1 & 0 & 0 \\ 0 & -1 & 1 & 0 & 0 & 0 & 0 & 0 & 0 & 0 & 0 & 1 & 0 & 1 & 0 \\ 0 & 0 & 0 & 0 & 0 & 0 & 1 & -1 & 0 & 0 & 1 & 0 & 1 & 0 & 0 \\ 0 & 1 & -1 & 0 & 0 & 0 & 0 & 0 & 0 & 0 & 0 & 1 & 0 & 1 & 0 \\ 0 & 0 & 0 & 0 & 0 & 0 & 0 & 0 & 0 & 0 & 0 & 0 & 0 & 0 & 1 \end{pmatrix}, \tag{21}$$

$$\text{and } \mathbf{T}_z = \begin{pmatrix} 0 & 0 & 0 & 0 & 0 & 0 & 0 & 0 & 0 & 0 & b & b & b & b & g \\ 0 & 0 & 0 & 0 & 0 & 0 & 0 & 0 & 0 & 0 & b & b & b & b & g \\ 0 & 0 & 0 & 0 & 0 & 0 & 0 & 0 & 0 & 0 & b & b & b & b & g \\ 0 & 0 & 0 & 0 & 0 & 0 & 0 & 0 & 0 & 0 & b & b & b & b & g \\ 0 & 0 & 0 & 0 & 0 & 0 & 0 & 0 & 0 & 0 & b & b & b & b & g \end{pmatrix}, \tag{22}$$

Notice that in (18), (20), and (22) all rows of the matrix are identical. This can be utilized to evaluate the AVM quantities $\zeta^i_{x,j,k}$, $\zeta^i_{y,j,k}$, and $\zeta^i_{z,j,k}$ utilizing (8) by:

$$\begin{aligned} \zeta^i_{x,j,k} &= \begin{bmatrix} \dfrac{\partial f_{3d}(\mathbf{p})}{\partial p_i} & \dfrac{\partial g_{3d}(\mathbf{p})}{\partial p_i} \end{bmatrix} \begin{pmatrix} 1 & 1 & 1 & 1 & 0 & \underline{\mathbf{0}}^T_{1\times 10} \\ 0 & 0 & 0 & 0 & 1 & \underline{\mathbf{0}}^T_{1\times 10} \end{pmatrix} \mathbf{V}^j_k \\ \zeta^i_{y,j,k} &= \begin{bmatrix} \dfrac{\partial f_{3d}(\mathbf{p})}{\partial p_i} & \dfrac{\partial g_{3d}(\mathbf{p})}{\partial p_i} \end{bmatrix} \begin{pmatrix} \underline{\mathbf{0}}^T_{1\times 5} & 1 & 1 & 1 & 1 & 0 & \underline{\mathbf{0}}^T_{1\times 5} \\ \underline{\mathbf{0}}^T_{1\times 5} & 0 & 0 & 0 & 0 & 1 & \underline{\mathbf{0}}^T_{1\times 5} \end{pmatrix} \mathbf{V}^j_k \\ \zeta^i_{z,j,k} &= \begin{bmatrix} \dfrac{\partial f_{3d}(\mathbf{p})}{\partial p_i} & \dfrac{\partial g_{3d}(\mathbf{p})}{\partial p_i} \end{bmatrix} \begin{pmatrix} \underline{\mathbf{0}}^T_{1\times 10} & 1 & 1 & 1 & 1 & 0 \\ \underline{\mathbf{0}}^T_{1\times 10} & 0 & 0 & 0 & 0 & 1 \end{pmatrix} \mathbf{V}^j_k \end{aligned} \tag{23}$$

Each sub-matrix leads to a single impulse to be stored for sensitivity analysis. The total required impulses for sensitivity calculation in the 3D case are 3 per cell per time step. This can be contrasted with the minimum storage of 15 per cell per time step as in the original TLM-based AVM technique.

In order to utilize the significant memory saving suggested by the impulse sampling, similar mathematical manipulation is done for the adjoint simulation. Also, in order to avoid any extra storage during

the AVM simulation, the adjoint variables are redefined as in (9) which is substituted in the original sensitivity calculation (3) to obtain the scalar summation (10). The original 30 memory storages per cell (15 for the original simulation and 15 for the adjoint simulation) are reduced to only three variables leading to 90% reduction in the storage cost. This reduction is associated with no computation overhead but rather reduces the computational cost.

4. NUMERICAL RESULTS

To validate our approach, we perform AVM sensitivity analyses of 3D problems. These problems include dielectric resonators in a parallel plate waveguide and a multi-segment dielectric resonator antenna (DRA). The sensitivity of the scattering parameters is estimated utilizing the developed impulse sampling algorithm. The results are verified by conducting expensive finite difference calculations.

4.1. Sensitivity Analysis for 3D Dielectric Resonators

Dielectric resonator filters have been exploited for ultra-sensitive microwave filters [18–20]. The simple tuning mechanisms have facilitated the application of such filters for base station transceivers [18]. In this example, dielectric resonant structures are embedded in a parallel plate waveguide (see Fig. 4). This structure is simulated as a full 3D structure. A complete list of the structure data and simulation parameters is included in Table 1.

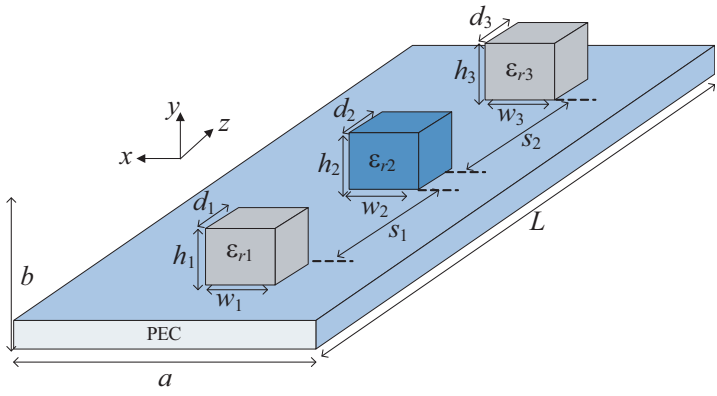

Figure 4. A dielectric resonator filter embedded inside a parallel plate waveguide.

Table 1. A list of the parameters utilized for the simulation and AVM calculations of the dielectric resonator structure.

Waveguide parameters			
$a = 40.0\,\text{mm}$	$b = 40.0\,\text{mm}$		$L = 100.0\,\text{mm}$
Dielectric posts parameters			
$d_1 = 20.0\,\text{mm}$	$w_1 = 15.0\,\text{mm}$	$h_1 = 10.0\,\text{mm}$	$\varepsilon_{r1} = 5$
$d_2 = 20.0\,\text{mm}$	$w_2 = 15.0\,\text{mm}$	$h_2 = 10.0\,\text{mm}$	$\varepsilon_{r2} = 5$
$d_3 = 20.0\,\text{mm}$	$w_3 = 15.0\,\text{mm}$	$h_3 = 10.0\,\text{mm}$	$\varepsilon_{r3} = 5$
Simulation parameters			
$\Delta l = 1.0\,\text{mm}$		No. of time steps $= 15,000$	
AVM memory requirement			
Conventional	1.26 Gigabytes	Impulse sampling	126 Megabytes

In this example, the wideband sensitivities of the S-parameters with respect to both material and geometrical properties are calculated. The vector of optimization variables $\mathbf{p} \in R^{14}$ is formulated as

$$\mathbf{p} = [d_1 \;\; w_1 \;\; h_1 \;\; d_2 \;\; w_2 \;\; h_2 \;\; d_3 \;\; w_3 \;\; h_3 \;\; \varepsilon_{r1} \;\; \varepsilon_{r2} \;\; \varepsilon_{r3} \;\; s_1 \;\; s_2] \tag{24}$$

where the dimensions of the resonators are d_i, w_i, h_i for $i = 1, 2$, and 3. The dielectric constant of the ith resonator is ε_{ri} and the spacing between the resonators is $s_1 = 10.0\,\text{mm}$, and $s_2 = 10.0\,\text{mm}$. The parallel plate waveguide structure, shown in Fig. 4, has the geometrical and material parameters shown in Table 1. The structure is excited using a plane wave excitation with a wide band Gaussian signal centered at $f = 5.0\,\text{GHz}$ with a bandwidth of $9\,\text{GHz}$. The utilized objective function is the scattering parameter S_{11}, which is a measure of the reflectivity of the resonator.

In this 3D problem, due to the memory efficiency of our algorithm, we can extend the regular AVM to the central AVM (CAVM) technique [21]. For CAVM calculation of sensitivities, we calculate the sensitivities with respect to shape parameters by perturbing the scattering matrix in both the forward and backward directions. Though negligible computational overhead is required, more accurate results are achieved [21]. In Figs. 5–7, the sensitivity calculations using the AVM are shown to have a good match with the finite difference approximations. The sensitivity is calculated with respect to 12 shape and material properties.

The memory requirement for sensitivity estimation using the original TLM-based AVM approach [15] can be calculated from the

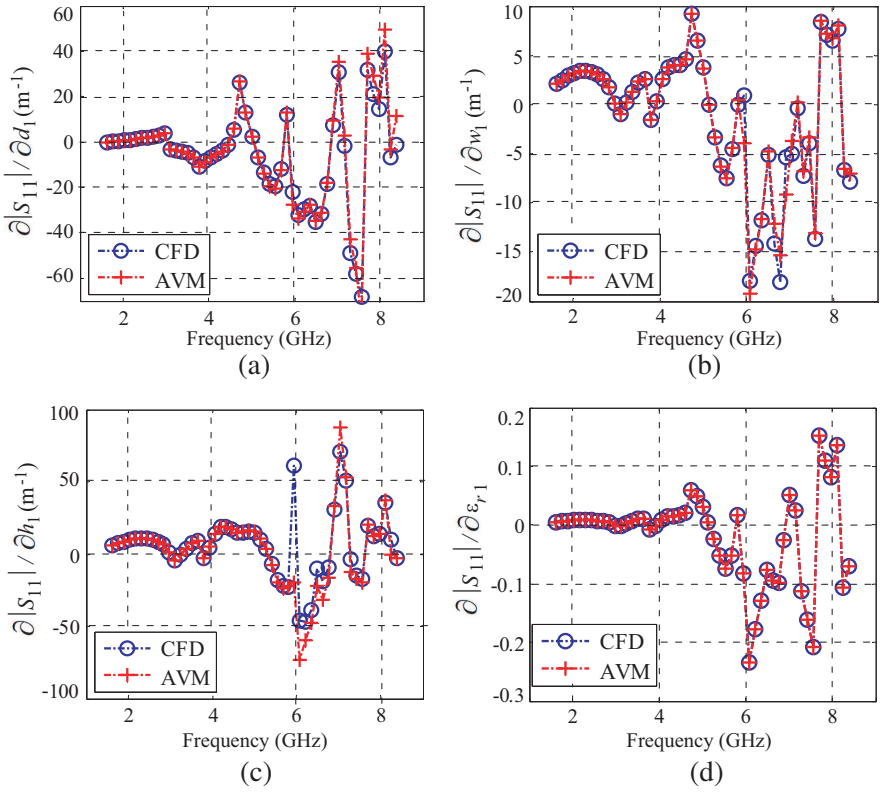

Figure 5. The return loss sensitivity with respect to the design parameters of the first dielectric post using the impulse sampling approach as compared to the central finite difference technique.

perturbation dimensions ($d \times w \times h$) for all embedded resonators and the numerical parameters. For the given structure dimensions, a total of $20 \times 15 \times 10$ cell vectors are stored at each instant. Each vector is of size 15 to account for the number of TLM link impulses. For a simulation time of 15000 time instants, required for wideband resonant structure simulation, the total of memory overhead is approximately 1.26 Gigabytes using conventional AVM approaches. Utilizing the impulse sampling technique, only 126 Megabytes are required.

4.2. Dielectric Resonator Antenna

We also illustrate our memory efficient approach through sensitivity analysis of the multi-segment dielectric resonator antenna (DRA) [22–

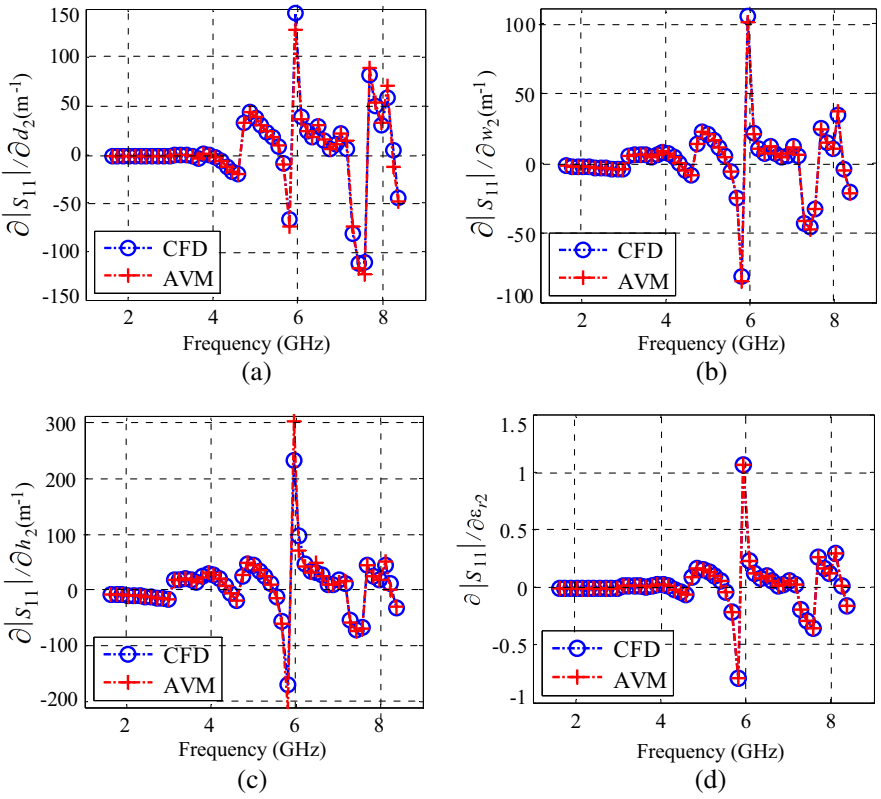

Figure 6. The return loss sensitivity with respect to the design parameters of the second dielectric post using the impulse sampling approach as compared to the central finite difference technique.

25] shown in Fig. 8. An inset of high permittivity dielectric material is included for feed matching as discussed in [22].

In this problem, we estimate the sensitivities of the frequency domain objective function $|S_{11}|$. The self adjoint algorithm is utilized leading to the calculation of the scattering parameters and its sensitivity for all the design parameters without performing any extra simulations. The design parameters are the dielectric permittivity of the antenna ε_r, the dielectric permittivity of the inset ε_i, and the dimensions w, d, h, and t. The specific design parameters along with the numerical constants are listed in Table 2.

The studied structure is a wide band antenna operating around a center frequency of 16.0 GHz with a relative bandwidth of approximately 20% [22]. The DRA is fed by a microstrip line of

Table 2. A list of the structure parameters utilized for the simulation and AVM calculations of the dielectric resonator antenna.

Structure parameters					
$\varepsilon_r = 10.0$	$\varepsilon_i = 20.0$	$w = 7.875\,\text{mm}$	$d = 2.0\,\text{mm}$	$h = 3.175\,\text{mm}$	$t = 0.6\,\text{mm}$
Simulation parameters					
$\Delta l = 0.2\,\text{mm}$		No. of time steps $= 2 \times 10^4$ time instants			
AVM memory requirement					
Conventional	16.5 Gigabytes		Impulse sampling		1.65 Gigabytes

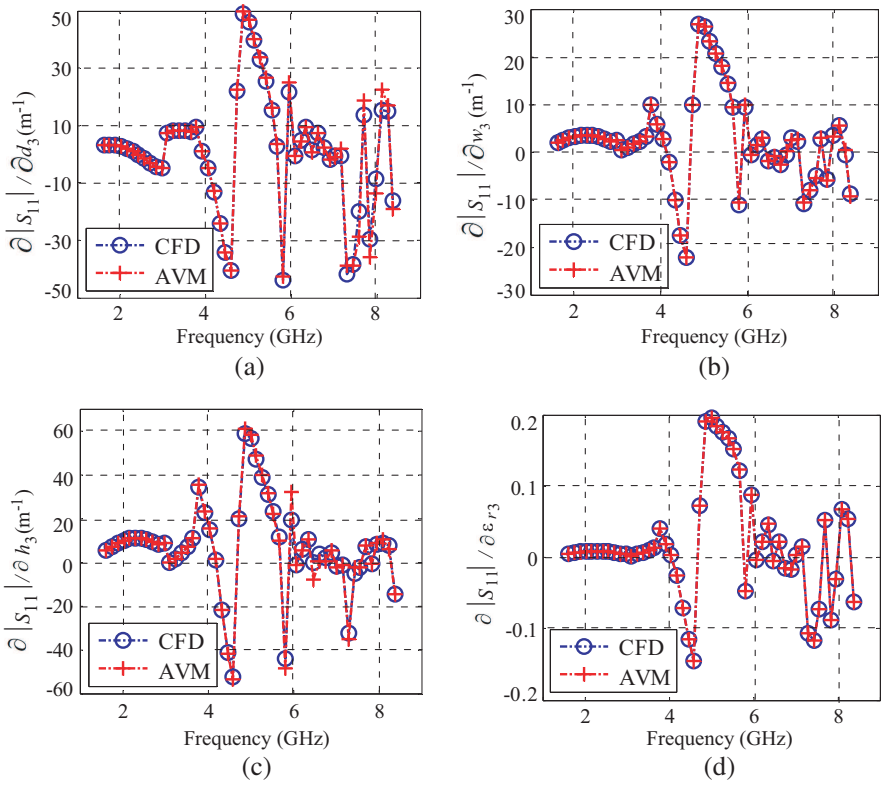

Figure 7. The return loss sensitivity with respect to the design parameters of the third dielectric post using the impulse sampling approach as compared to the central finite difference technique.

width = 1.9 mm over a dielectric substrate of relative permittivity $\varepsilon_{sub} = 3.0$ and thickness $h_{sub} = 0.762\,\text{mm}$. The DRA is designed of a material with $\varepsilon_r = 10.0$. The design dimensions are shown in

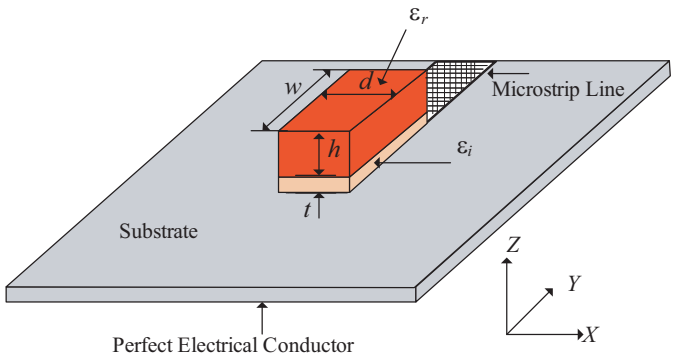

Figure 8. The multisegment dielectric resonator antenna.

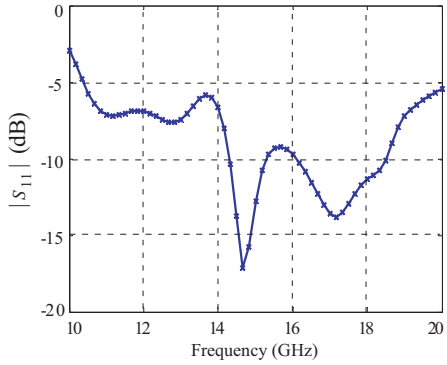

Figure 9. The estimated return loss for the DRA antenna simulated by an in house TLM code with $\Delta l = 0.2\,\text{mm}$.

Table 2. A dielectric inset is included to allow for wide band impedance matching. It is made from a ceramic of relative permittivity $\varepsilon_i = 20.0$ and thickness $t = 0.6\,\text{mm}$.

The structure is simulated using our in-house TLM code in order to estimate the return loss (S_{11}) and its sensitivities using our memory efficient technique. The utilized spatial step size is $\Delta l = 0.2\,\text{mm}$. The return loss of the structure (see Fig. 9) is in good agreement with the results in [22]. The sensitivities of the return loss with respect to the DRA and inset material properties are shown in Figs. 10 and 11. Shown in Figs. 12–15 are the sensitivities of the return loss with respect to the dimensional parameters. The AVM results are in good agreement with the results obtained using the finite difference techniques. In Fig. 15, the slight deviation of the AVM results from central finite difference results is attributed to the high nonlinear dependence of the objective function on the inset thickness. This can be illustrated by estimating

the forward and backward finite difference sensitivities (FFD, BFD).

For the studied design parameters (ε_r, ε_i, w, d, h, t), the finite difference approaches require extra twelve simulations for sensitivity calculations. The regular AVM technique for TLM requires a large memory overhead. For the DRA example a domain of size $10\Delta l \times 19\Delta l \times 39\Delta l$ is perturbed. The simulation requires 2×10^4 time instants

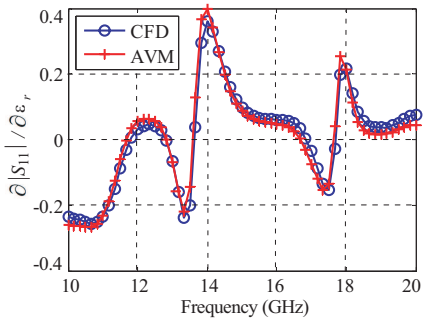

Figure 10. The return loss sensitivity with respect to the dielectric constant of the DRA at $\Delta l = 0.2$ mm using the impulse sampling approach as compared to the central finite difference technique.

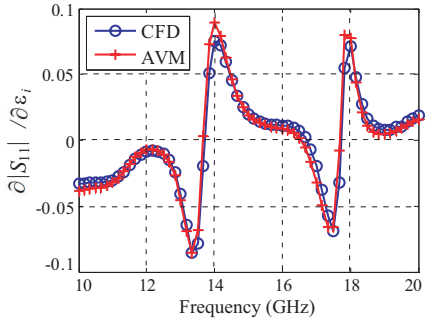

Figure 11. The return loss sensitivity with respect to the dielectric constant of the inset of the DRA at $\Delta l = 0.2$ using the impulse sampling approach as compared to the central finite difference technique.

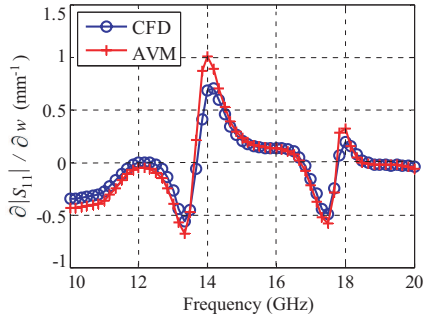

Figure 12. The return loss sensitivity with respect to the dimension w of the DRA for $\Delta l = 0.2$ mm using the impulse sampling approach as compared to the central finite difference approximation.

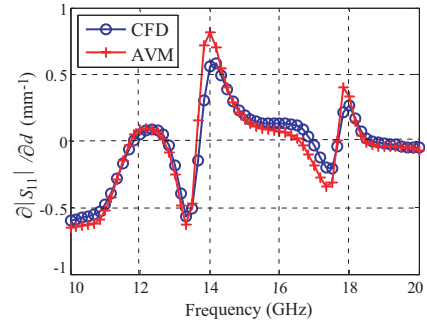

Figure 13. The return loss sensitivity with respect to the dimension d of the DRA for $\Delta l = 0.2$ mm using the impulse sampling approach as compared to the finite difference approximation.

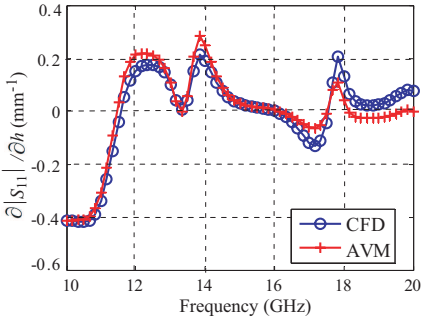

Figure 14. The return loss sensitivity with respect to the DRA height h for $\Delta l = 0.2$ mm using the impulse sampling approach as compared to the finite difference approximation.

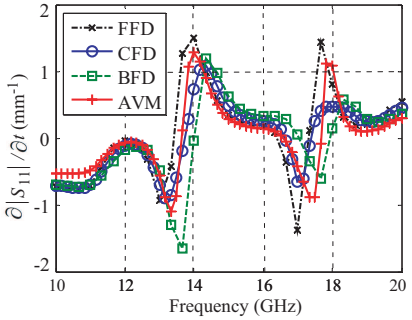

Figure 15. The return loss sensitivity with respect to the inset thickness t for $\Delta l = 0.2$ mm using the impulse sampling approach as compared to the finite difference approximations.

to accurately calculate the wideband scattering parameters. The overall memory overhead for regular AVM technique is 16.5 Gigabytes. Our memory efficient AVM technique requires only 1.65 Gigabytes memory overhead. This order of magnitude reduction allows for the sensitivity calculation of 10 times larger perturbations.

5. CONCLUSIONS

We propose an efficient approach for the TLM-based AVM sensitivities. Using an elegant manipulation of the scattering and connection matrices, the required storage of the approach is reduced to only 20% of its original value. By eliminating the storage of the adjoint field and estimating all sensitivities on the fly, the required storage is further reduced to only 10% of its original value. Our approach is illustrated through two 3D examples with extensive memory storage. Very good agreement is achieved between our impulse sampling sensitivity approach and the finite difference approaches.

REFERENCES

1. Ghaffari-Miab, M., A. Farmahini-Farahani, R. Faraji-Dana, and C. Lucas, "An efficient hybrid swarm intelligence-gradient optimization method for complex time Green's functions of multilayer media," *Progress In Electromagnetics Research*, Vol. 77, 181–192, 2007.

2. Chung, Y., J. Ryu, C. Cheon, I. Park, and S. Hahn, "Optimal design method for microwave device using time domain method and design sensitivity analysis — Part I: FETD case," *IEEE Trans. Magn.,* Vol. 37, 3289–3293, 2001.
3. Chung, Y., C. Cheon, I. Park, and S. Hahn, "Optimal design method for microwave device using time domain method and design sensitivity analysis — Part II: FDTD case," *IEEE Trans. Magn.,* Vol. 37, 3255–3259, 2001.
4. Radwan, A. G., M. H. Bakr, and N. K. Nikolova, "Transient adjoint sensitivities for discontinuities with gaussian material distributions," *Progress In Electromagnetics Research B*, Vol. 27, 1–19, 2011.
5. Basl, P. A. W., M. H. Bakr, and N. K. Nikolova, "Efficient transmission line modeling sensitivity analysis exploiting rubber cells," *Progress In Electromagnetics Research B*, Vol. 11, 223–243, 2009.
6. Ahmed, O. S., M. H. Bakr, and X. Li, "A memory-efficient implementation of TLM-based adjoint sensitivity analysis," *IEEE Trans. Antennas Propagat.*, Vol. 60, 2122–2125, 2012.
7. Bakr, M. H. and N. K. Nikolova, "An adjoint variable method for time-domain transmission line modeling with fixed structured grids," *IEEE Trans. Microw. Theory Tech.*, Vol. 52, 554–559, 2004.
8. Nikolova, N. K., H. W. Tam, and M. H. Bakr, "Sensitivity analysis with the FDTD method on structured grids," *IEEE Trans. Microw. Theory Tech.*, Vol. 52, 1207–1216, 2004.
9. Bakr, M. H. and N. K. Nikolova, "An adjoint variable method for frequency domain TLM problems with conducting boundaries," *IEEE Microw. and Wireless Components Lett.*, Vol. 13, 408–410, 2003.
10. Georgieva, N. K., S. Glavic, M. H. Bakr, and J. W. Bandler, "Feasible adjoint sensitivity technique for EM design optimization," *IEEE Trans. Microw. Theory Tech.*, Vol. 50, 2751–2758, 2002.
11. Webb, J. P., "Design sensitivity of frequency response in 3-D finite-element analysis of microwave devices," *IEEE Trans. Magn.,* Vol. 38, 1109–1112, 2002.
12. Basl, P. A. W., M. H. Bakr, and N. K. Nikolova, "Theory of self-adjoint S-parameter sensitivities for lossless nonhomogeneous transmission-line modeling problems," *IET Microwave Antennas Propag.*, Vol. 2, 211–220, 2008.
13. Johns, P. B., "A symmetrical condensed node for the TLM

method," *IEEE Trans. Microw. Theory Tech.*, Vol. 35, 370–377, 1987.

14. Hoefer, W. J. R., "The transmission-line matrix method — Theory and applications," *IEEE Trans. Microw. Theory Tech.*, Vol. 33, 882–893, 1985.
15. Basl, P. A. W., M. H. Bakr, and N. K. Nikolova, "An AVM technique for 3D TLM with symmetric condensed nodes," *IEEE Microw. and Wireless Components Lett.*, Vol. 15, 618–620, 2005.
16. Trenkic, V., C. Christopoulos, and T. M. Benson, "New symmetrical super-condensed node for the TLM method," *Electronics Lett.*, Vol. 30, 329–330, 1994.
17. Paul, J., C. Christopoulos, and D. W. P. Thomas, "Generalized material models in TLM — Part I: Materials with frequency-dependent properties," *IEEE Trans. Antennas Propagat.*, Vol. 47, 1528–1534, 1999.
18. Mansour, R. R., "High-Q tunable dielectric resonator filters," *IEEE Microw. Mag.*, Vol. 10, 84–98, 2009.
19. Cohn, S. B., "Microwave bandpass filters containing high-Q dielectric resonators," *IEEE Trans. Microw. Theory Tech.*, Vol. 16, 218–227, 1968.
20. Saliminejad, R. and M. R. Ghafouri Fard, "A novel and accurate method for designing dielectric resonator filter," *Progress In Electromagnetics Research B*, Vol. 8, 293–306, 2008.
21. Ali, S., N. Nikolova, and M. H. Bakr, "Central adjoint variable method for sensitivity analysis with structured grid electromagnetic solvers," *IEEE Trans. Magn.,* Vol. 40, 1969–1971, 2004.
22. Petosa, A., N. Simons, R. Siushansian, A. Ittipiboon, and M. Cuhaci, "Design and analysis of multisegment dielectric resonator antennas," *IEEE Trans. Antennas Propagat.*, Vol. 48, 738–742, 2000.
23. Rezaei, P., M. Hakkak, and K. Forooraghi, "Design of wide-band dielectric resonator antenna with a two-segment structure," *Progress In Electromagnetics Research*, Vol. 66, 111–124, 2006.
24. Al-Zoubi, A. S., A. A. Kishk, and A. W. Glisson, "Analysis and design of a rectangular dielectric resonator antenna FED by dielectric image line through narrow slots," *Progress In Electromagnetics Research*, Vol. 77, 379–390, 2007.
25. Fayad, H. and P. Record, "Multi-feed dielectric resonator antenna with reconfigurable radiation pattern," *Progress In Electromagnetics Research*, Vol. 76, 341–356, 2007.